

An ASME-Compliant Helium-4 Evaporation Refrigerator for the SpinQuest Experiment

Jordan D. Roberts*, Vibodha Bandara*[†], Kenichi Nakano *, Dustin Keller *

*University of Virginia, Charlottesville, VA, USA

[†]University of Colombo, Colombo, Sri Lanka

Abstract—This paper presents the design, safety basis, and commissioning results of a 1 K liquid helium-4 (^4He) evaporation refrigerator developed for the Fermilab SpinQuest Experiment (E1039). The system represents the first high-power helium evaporation refrigerator operated in a fixed-target scattering experiment at Fermilab and was engineered to comply with the Fermilab ES&H Manual (FESHM) requirements governing pressure vessels, piping, cryogenic systems, and vacuum vessels. The design is mapped to ASME B31.3 (Process Piping) and the ASME Boiler and Pressure Vessel Code (BPVC) for pressure-boundary integrity and overpressure protection, with documented compliance to FESHM Chapters 5031 (Pressure Vessels), 5031.1 (Piping Systems), and 5033 (Vacuum Vessels). This work documents the methodology used to reach compliance and approval for the ^4He evaporation refrigerator at Fermilab which the field lacks. Design considerations specific to the high-radiation target-cave environment—including remotely located instrumentation approximately 20 m from the cryostat—are summarized, together with the relief-system sizing methodology used to accommodate transient heat loads from dynamic nuclear polarization microwaves and the high-intensity proton beam. Commissioning data from July 2024 confirms that the system satisfies all thermal-performance and safety objectives.

Index Terms—Spin physics, polarized target, helium refrigeration, cryogenics, process piping, ASME B31.3, ASME BPVC, FESHM compliance.

I. INTRODUCTION

SpinQuest (E1039) at Fermilab employs a high-cooling-power liquid helium-4 (^4He) evaporation refrigerator integrated with a superconducting magnet and operated within a high-radiation target cave. The system is required to maintain sub-4 K temperatures at the polarized target while accommodating large, rapidly varying heat loads generated by dynamic nuclear polarization microwaves (DNP) and by the high-intensity 120 GeV proton beam (up to 10^{13} protons per 4-second spill). These operational demands, combined with stringent laboratory safety requirements for pressure vessels, piping, and cryogenic systems, necessitated a robust and compliant design. The resulting system features substantial margins relative to ASME code allowables, robust overpressure protection, and radiation-hardened remote instrumentation and controls.

Dynamically polarized targets play a critical role in high-energy and nuclear scattering experiments, enabling precision measurements of spin-dependent observables starting with the work from Abragam [1][2][3] and Borghini [4][5]. Experiments such as E155 at Stanford Linear Accelerator Center

(SLAC) [6] or Jefferson Lab CLAS [7], used an electron beam with a ^4He evaporation refrigerator, to obtain high polarization in target material such as solid ^6LiD , NH_3 , or ND_3 . As experimental facilities advanced toward higher beam intensities and energy domains, the demand for target systems capable of operating at higher temperatures with greater cooling capacity led to the widespread adoption of ^4He evaporation refrigerators. These systems provide cooling powers in the watt range—one to two orders of magnitude higher than earlier ^3He or dilution refrigerators—while maintaining operating temperatures near 1 K as illustrated by later experiments at Brookhaven National Lab and Jefferson Lab [8], [9], [10].

In modern fixed-target experiments, the engineering and safety requirements for cryogenic systems have evolved along with these performance needs. Laboratories funded by the Department of Energy over time have expanded their compliance with institutional safety standards, an example of this is the Fermilab ES&H Manual (FESHM) [11], which references the ASME Boiler and Pressure Vessel Code (BPVC) Section VIII and ASME B31.3 Process Piping standards [12]. Because these codes were originally developed for high-pressure, high-temperature industrial systems, their direct application to low-pressure cryogenic vessels requires conservative adaptation of ASME [12], as facilities such as CERN found out [13]. Recent projects in national accelerator facilities, such as the Jefferson Lab’s programs [14], [15], [16], have demonstrated the viability of applying ASME principles to cryogenic refrigeration systems. However, comprehensive documentation of the underlying design methodology and compliance process remains limited.

Motivated by the need for a documented, standards-compliant design applicable to high-radiation environments, the University of Virginia (UVA) Spin Physics Group developed a ^4He evaporation refrigerator for the SpinQuest (E1039) experiment. The system integrates with a 5 T superconducting magnet and supports continuous DNP operation under high-intensity, high energy proton beam conditions.

This paper presents the design methodology, safety basis, and commissioning performance of the UVA ^4He evaporation refrigerator for the SpinQuest experiment. Section II describes the design geometry and illustrates the purpose of each component in the refrigeration system. Section III covers the application of the FESHM and code to prepare the system for use at Fermilab. In this section, the maximum allowed working pressure (MAWP) is calculated, and overpressure relief is cov-

ered. Section IV reviews the results from the commissioning of the polarized target at Fermilab, confirming its accepted use. Section V summarizes and reinforces the application of the code. Finally, Section VI concludes with lessons learned and implications for future high-intensity polarized-target systems.

II. SYSTEM OVERVIEW

The 1 K liquid ^4He evaporation refrigerator, shown schematically in Fig. 1, comprises a vacuum-insulated shell and nose assembly that houses the evaporative stage. A stainless-steel annular helium phase separator is positioned at the top of the cryostat and thermally isolated from the external environment using multiple perforated copper baffles. Liquid ^4He from the separator is directed through the lower heat exchanger before entering the nose reservoir, where the 120 GeV proton beam passes through the beam window and interacts with the solid-state cryogenic target. A CryoFab 316L stainless-steel U-tube jumper transfers the liquid ^4He stored in the superconducting magnet dewar to the separator, providing the liquid helium supply.

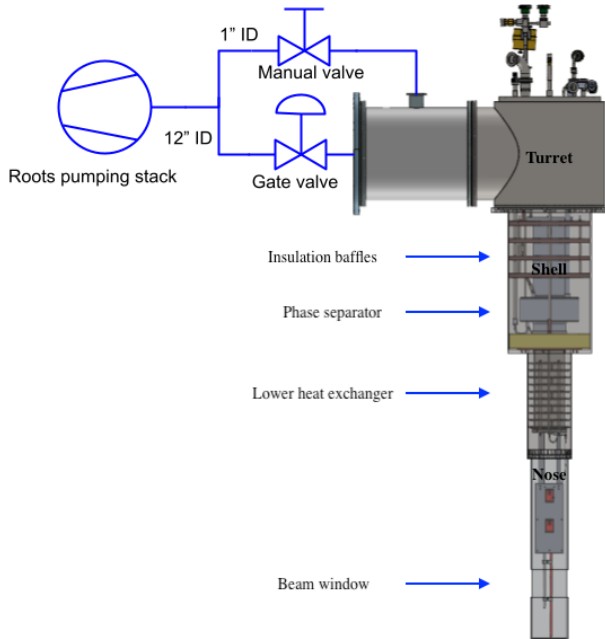


Fig. 1: Simplified schematic of the refrigerator system showing the major components and connections to the pumping stack through the gate valve and bypass line. Arrows indicate key features within the shell–nose assembly.

System overpressure protection is achieved through a 3 psig spring-loaded relief valve installed on the separator discharge and a parallel-plate relief device on the common vent line. Exhaust handling and cryogenic pumping are provided by a stack of Roots and diaphragm pumps, which together supply the required mass-flow rate for stable 1 K operation. The design calculations and choices for the relief lines are further discussed in Section III-B.

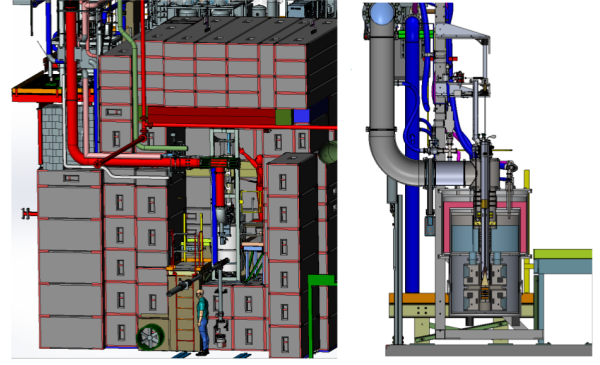


Fig. 2: Shown is the target within the high radiation-shielded enclosure, left, and a zoom in on the refrigerator placement within the polarized target, right.

Due to the high energy of the experiment, special requirements are needed to meet the Fermilab radiation safety assessment criteria. Consequently, the polarized target cryostat is situated within a radiation-shielded enclosure, called the target cave, which is shown in Fig. 2.

The enclosure is constructed from dense shielding blocks to attenuate secondary radiation from both beam–target and beam–dump interactions, confining activation to the immediate vicinity of the target. All silicon-based instrumentation is routed outside the target enclosure to mitigate radiation-induced degradation and allow remote operation. Electronics placed within approximately one meter of the target would otherwise experience mixed-field radiation levels on the order of 10^3 Gy(Si) total ionizing dose and hadron influences approaching 10^{12} cm^{-2} (1 MeV neutron equivalent) over a three-month running period—sufficient to induce severe single-event effects and cumulative damage in most silicon-based devices within only a few hours of operation. The safety design choices of radiation-hardened control valves are discussed in Section III.

The following subsections detail the several components of the ^4He evaporation refrigerator. This section is focused on the geometric design and physical requirements of the experiment. For a detailed review of the application of the code, see Section III.

A. Shell and Nose Assembly (Vacuum Vessel)

The shell and nose assembly provides the high-vacuum insulated barrier and structural support for the refrigerator internals, which make up the refrigerator space. The shell bolts to the top flange of the 5 T superconducting magnet functioning as the internal wall of the insulating vacuum chamber, which is continuously pumped down with a set of turbo molecular pumps during operation to below 10^{-7} Torr. The turret connects the pump stack and the refrigerator space by sealing onto the top flange of the shell with bolts. The refrigerator is bolted onto the top flange of the turret, positioned along the vertical axis of the magnet. The target insert passes through the center bore of the assembly and has a

ladish flange and clamp that seals to the top of a bellows line connecting to the top flange of the refrigerator. The total assembly length is 46.7 in, with a top flange diameter of 12.6 in tapering to 4.8 in, allowing the phase separator to seat along the vertical axis of the magnet bore. These dimensions are dictated by the 5 T superconducting magnet geometry, to which the refrigerator cryostat must directly couple. The channel through the refrigerator is 2.5 cm by 8 cm to accommodate the polarized target cell.

Material selection prioritized manufacturability, thermal performance, and compliance for the shell and nose. The shell was fabricated from rolled 304 stainless steel sheets joined by fusion welds, while the nose was machined from a solid rod of aluminum 6061-T6. The two were bolted together and sealed using an indium gasket to ensure vacuum integrity at low temperatures. These design choices provided a realistic assembly that best aligns with the goals of the experiment and aids in compliance with the FESHM.

As a cryostat, the nose maintains the helium liquid level while incorporating the thinnest section of the system, a 0.013 in precision beam window. This beam window forms the interface between the polarized target material and the incident 120 GeV proton beam, making it a critical component for SpinQuest target operation. The external surface is wrapped in layers of Mylar and a webbed mesh to reduce conductive and radiative heat leaks. The entire assembly can be lifted from the magnet using approved fixtures for maintenance.

B. U-Tube Jumper

The U-tube, fabricated by Cryofab, serves as a low-resistance vacuum-insulated transfer path for liquid helium from the magnet dewar to the phase separator. The U-tube mates to the magnet dewar and phase separator via a compression fitting, ensuring leak-tight operation. The U-tube, constructed from 316L stainless steel, has an inner diameter of 0.188 in and a wall thickness of 0.016 in. Based on ASME B31.3 process piping formulas, the vendor-specified theoretical MAWP is 3648 psig, far exceeding the operating envelope of the SpinQuest refrigerator. Given the extreme margin between the calculated MAWP and expected normal operating pressures of 13.8 psig, the U-tube is considered code-compliant with ASME B31.3 and well within FESHM pressure-systems requirements [11]. The vacuum is created using a vacuum valve and a pump-out operator. This valve not only seals the insulation vacuum but also acts as a relief. The relief path of the U-Tube line is discussed in Section III-B.

C. Phase Separator and Cold Insulation Baffles

Seated at the base of the shell is the annular phase separator (separator) that provides the first stage of precooling and manages the liquid-vapor mixture transferred by the U-Tube from the magnet dewar. This is critical as during operation, liquid helium transferred from the magnet dewar partially evaporates, forming a two-phase mixture. This flow passes through a sintered copper plate with 50 μm porosity and 1 mm thickness that divides the separator into two chambers. The

sintered plate, manufactured from Electrolytic Tough Pitch (ETP) copper powder, provides high thermal conductivity and large surface area, enabling efficient vapor-liquid separation and precooling of the remaining liquid through evaporation. The fabrication of the sintering plate and design is detailed by Tapio's work, [17][18]. A model of the separator with the sintered plate exposed is shown in Fig. 3.

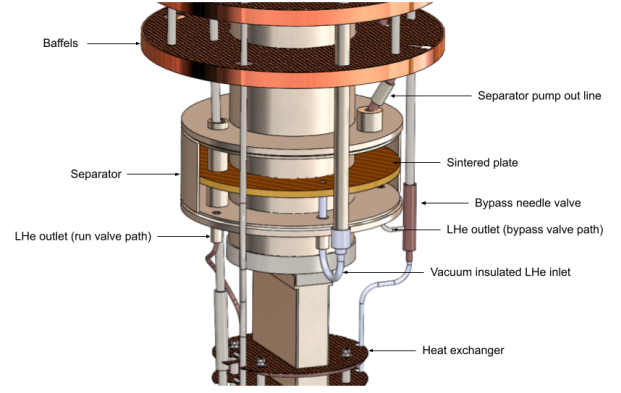


Fig. 3: A cross-sectional view of the phase separator showing the baffles above and the liquid helium path.

As the vapor and liquid separate, a diaphragm pump removes the helium vapor from the separator to exhaust it upward across the radial perforated copper baffles that are in thermal contact with the central bore of the refrigerator and shell wall. These baffles act as a cold radiation shield, reducing environmental heat ingress. Thermal modeling using equation 1 using the specific heat, c , of helium at 4 K, indicates that the baffles offset an estimated 7 W heat load from the environment to the helium liquid in the separator and the nose.

$$\dot{Q} = mc\Delta T \quad (1)$$

Pumping on the separator not only handles the vapor but lowers the liquid temperature, thereby establishing the sub-4 K environment required for the subsequent evaporative stage. The outer diameter of the separator is 6.4 in and the inner diameter is 3.6 in. All but the sintered plate was fabricated from 316L stainless steel with fused welds to fit concentrically around the polarized target insert at the level of the shell's base. This close fit directs the exhaust flow path up through the perforated copper baffles, aiding in the cold insulation layer. Helium flows from the underside of the separator, through the sintered plate to exit onto its surface. The upper insulated baffles and lower heat exchanger piping connect to the separator top plate and bottom plate. In general, all stainless-to-stainless joints are fusion-welded, while copper-to-stainless interfaces are made using silver solder. This jointing method is standard in rapid-cycling helium refrigerators and provides mechanical compliance to accommodate thermal contraction during repeated cooldown and warm-up cycles.

As mentioned above, the separator directly connects to the magnet dewar via the U-Tube line. Because of this, the

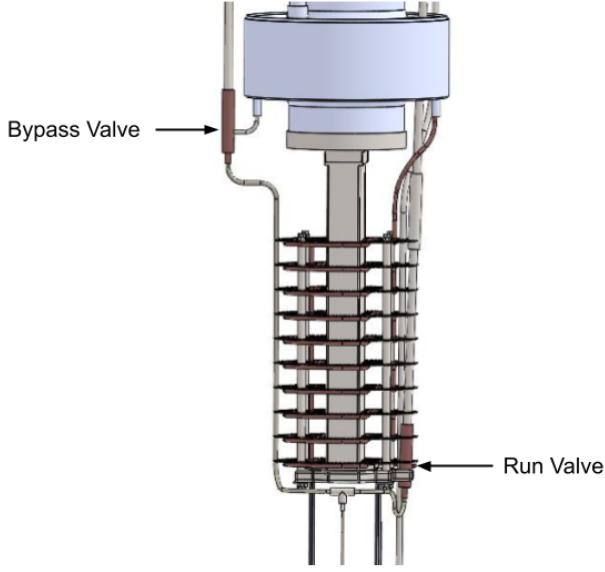


Fig. 4: The above model shows the valve location of the run and bypass helium routes. The run and bypass needle valves are remotely controlled. The Bypass valve reroutes liquid from the separator to the nose for fast filling. The run valve allows for throttling of the separator pre-cooled liquid through the lower heat exchanger and to the nose.

credible overpressure scenarios (quench return, blocked vent, or vacuum loss) and relief are discussed in Section III-B. The MAWP calculation was done and is detailed in Section III-A2.

D. Lower Heat Exchanger

The pre-cooled liquid from the first precooling stage moves down to the lower heat exchanger, where it enters the nose. The lower heat exchanger provides the second stage of precooling, where sub-4 K liquid helium from the phase separator is further cooled by ~ 1 K vapor returning from the nose. Liquid flow into the exchanger is regulated by a precision needle valve, while a parallel bypass needle valve, which allows for rapid filling of the nose volume when required, as shown in Fig. 4.

To improve heat transfer, the coiled tubing is thermally anchored to several perforated copper baffles, similar in design to the cold insulation baffles described in the prior Section II-C. These baffles increase surface area that promotes uniform cooling and reduces heat leaks from the shell wall. The exchanger itself consists of 0.10 in diameter stainless-steel tubing, extending 11.4 in from the separator and coiled concentrically around the polarized target insert. Paired with the separator, this precooling phase offers thermal stability. The primary cooling power during target operation is provided by the high volumetric flow of the Roots pump stack, which lowers the vapor pressure in the nose to approximately 1 K.

E. Pumps and Root Piping

The high volumetric flow of the root pump stack drives the cooling power of the refrigerator by quickly lowering the pressure on the helium bath. As the pressure drops, the vapor pressure increases due to the high evaporation of liquid helium within the nose and removes the heat from the polarized target sample. By doing so, the liquid temperature is maintained near 1 K, enabling sufficient cooling power for target operation as described by Tapio [17].

The pump stack consists of two WHU 7000 roots blowers operating in parallel as the first stage ($16,800 \text{ m}^3/\text{h}$ at 60 Hz), a single WHU 7000 as the second stage ($8,400 \text{ m}^3/\text{h}$), and an SV630 rotary vane backing pump ($756 \text{ m}^3/\text{h}$). The ideal volumetric flow is $10,080 \text{ m}^3/\text{h}$ at 0.1 mbar; however, the effective pumping speed is reduced by conductance limitations in the root piping. Table I summarizes the stack specifications.

TABLE I: Pump stack configuration and capacities

Stage	Pump Type	Model	Capacity (m^3/h)
1	Roots blower (parallel)	2 \times WHU 7000	16,800
2	Roots blower	WHU 7000	8,400
3	Rotary vane	SV630	756

The root piping connects the 1 K cryostat to a vertically oriented intermediate reservoir, followed by a right-angle connection to a large turret. Added conductance from the roots piping reduces the effective pumping speed relative to the ideal. The design of the piping was motivated to place the pump stack outside of the high radiation zone of the target cave. However, the stack design, in combination with the piping geometry, still satisfies the conductance and flow requirements dictated by the SpinQuest polarized target experiment. While the pump stack and associated piping contribute to the overall helium handling and cooling, the present work is limited to the design, safety, and commissioning of the refrigerator itself.

F. Instrumentation and Remote Location

As mentioned above, the target cave can expose equipment to $10^3 \text{ Gy}(\text{Si})$ total ionizing dose. The high radiation can degrade equipment and cause failures in semiconductor systems. To minimize radiation exposure and facilitate maintenance, all active instrumentation, including pressure transducers and manometers, was located outside the target cave, approximately 20 m from the cryostat. Radiation-resistant elastomer seals were employed, and a periodic replacement plan is specified to ensure long-term reliability. Signals were conveyed through a stainless-steel 1/4 in sensing line terminated with KF-16 fittings. The line is stagnant and classified as Category D service; when constructed from components with vendor ratings above 15 psig, this configuration complies with FESHM 5031.1 [11], without requiring a formal engineering note. Leak checks follow Fermilab's low-stress piping practice and are scheduled periodically. Although most instruments are outside the cave, some must be within the radiation environment, such as the target insert. As so, the insert requires a special procedure to move and radiation-harden sensors.

G. Target Insert

The target insert, shown in Fig. 5, is placed along the central axis of the refrigerator and contains three target cells to hold target material. Each cell, oval in shape, 8 cm long, is made of polychlorotrifluoroethylene (PCTFE) material. This choice was made on the basis of PCTFE properties at low temperatures and radiation hardness. To ensure precise measurements, each cell has three NMR inductor coils for polarization monitoring and three-chip resistors to map the microwave profile along its length using a temperature change. Cernox sensors are placed in both the top and bottom cells to precisely measure the temperature of the target materials. This accurate temperature monitoring plays a critical role in optimizing the annealing process that removes added unpaired electrons obtained during operation. The insert has a total length of 64.5 inches, with the assembly's body constructed from carbon fiber to minimize thermal conductivity. The top flange of the insert is a 4-inch sanitary blank flange, which contains SMA connectors for the NMR, a microwave waveguide connection, and connectors for the chip resistors and Cernox sensors. A gold-plated microwave horn is positioned just above the target cell assembly to emit microwaves to the target cells submerged in liquid helium.

A close-up on the target housing is shown in Fig. 5 showing the target cells, microwave horn, fridge-nose and the 0.25mm beam window on the nose and the beam path.

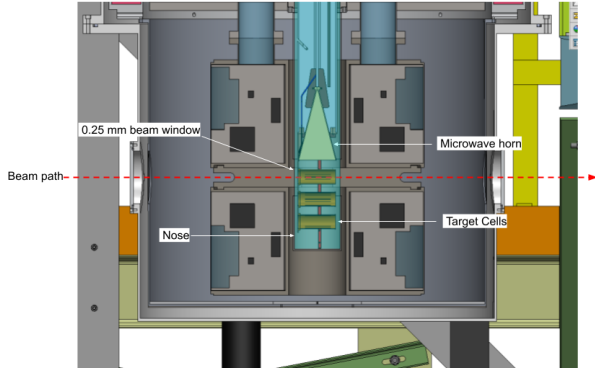


Fig. 5: A model zoomed in the target housing of the insert along the central axis of the refrigerator. A microwave horn is label delivering the 140 GHz to the target cells. Three target cells are shown with NMR loops inside. The beamline, shown as a red dashed line, passes through the beam window to interact with the target. All three target cells are submerged within liquid helium.

This insert enables consistent DNP in a high radiation zone and provides the necessary measurement for the experiment. A common measurement is done during minimal polarization at thermal equilibrium. To achieve this, control valves are required for a stable temperature within the cryostat.

H. Control Valve Actuation

The liquid helium delivery to the refrigerator nose occurs via two paths, as mentioned in Section II-D: a bypass valve

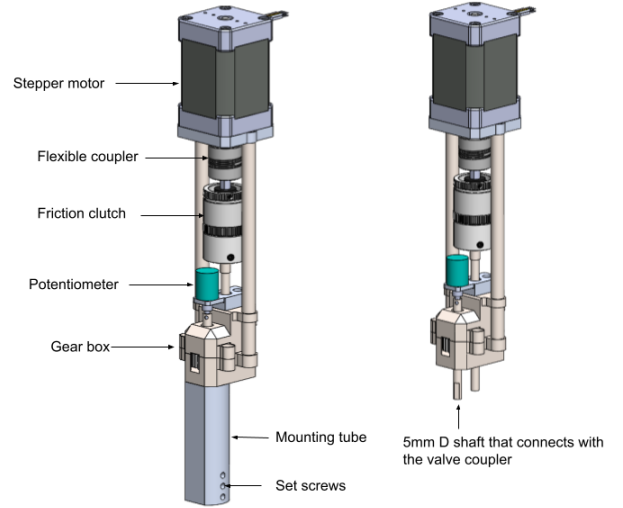


Fig. 6: The run valve assembly includes a custom gearbox, friction clutch, and rotary potentiometer. The design offsets the motor from the vertically moving target ladder and mounts to the run valve shaft using three 8-32 set screws. A rotary potentiometer provides absolute valve position feedback. The right side image shows the 5 mm D shaft

for rapid cooldown and a run valve for steady-state operation through the heat exchanger. Both valves, shown in Fig. 4, are Oxford Instruments needle valves, operated remotely due to radiation and access constraints.

The primary design challenges were: (1) avoiding refrigerator overflow, which risks brittle failure of magnet vacuum seals; and (2) mitigating spatial interference with the target ladder and insert path. To address these challenges, a NEMA 17 stepper motor with a friction clutch and flexible coupler was selected to regulate torque (0.4 Nm closing load). As well, a custom stainless-steel spur gearbox (1.25:1 ratio) offsets the motor assembly from the ladder path. Absolute position feedback is provided by a rotary potentiometer, chosen for radiation tolerance.

The bypass valve required a horizontal layout to preserve target insert clearance. Therefore, a worm drive (10:1 ratio) was used to redirect the motion, coupled through a friction clutch and potentiometer. Detailed in Fig. 6 is a model of the assembly for the run valve, with the design of the bypass valve being similar.

Both actuators were simulated for mechanical failure at the maximum motor torque (without clutch slip) as shown in Fig. 7, and tested to ensure radiation-hard feedback, ensuring safe operation despite limited access. This analysis was conducted to evaluate the mechanical stability of the actuator under extreme conditions and to validate the design's safety margin.

The third control valve is the gate valve bypass and is the most critical. This valve provides stable refrigerator operation through precise regulation of helium vapor pumping speed during thermal equilibrium measurements. The refrigerator

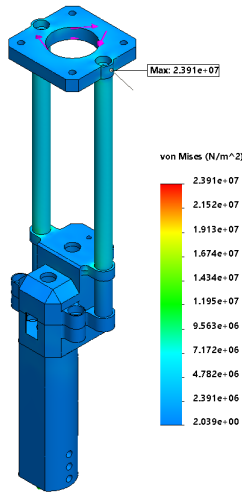


Fig. 7: Maximum von Mises stress and displacement of the run valve under the worst-case loading scenario, simulated using SolidWorks for 304 stainless steel.

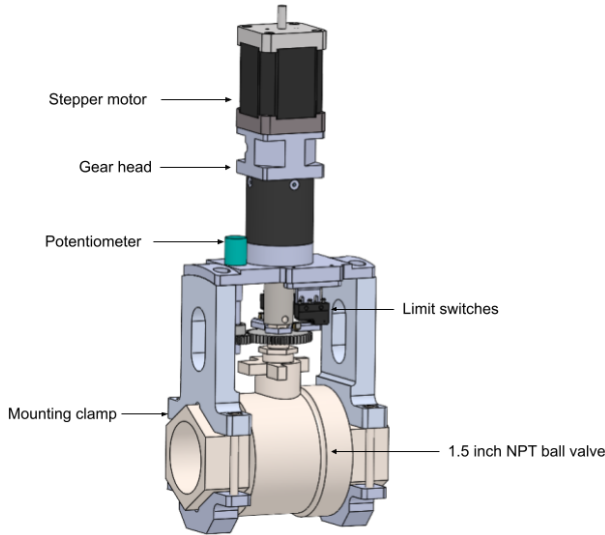


Fig. 8: Gate valve bypass actuator incorporating a 1:32 gear-box with stepper motor, rotary potentiometer for position feedback, and two limit switches for travel limits

connects to the Roots pumping stack via two parallel paths: a 12 in low-impedance gate valve for high-speed pumping, and a 1 in high-impedance line with a motorized valve for fine control. The actuator employs a stepper motor with a 1:32 planetary gearhead, potentiometer feedback, and snap-action limit switches at travel limits. A model of the remote gate valve bypass is illustrated in Fig. 8.

I. Control System Architecture

Control of all valves was implemented in LabVIEW, where the valve position is modulated by a PID loop using helium vapor pressure as the process variable. Pressure measurements

are provided by a Baratron manometer, cross-referenced with NIST He-4 vapor pressure–temperature correlations enabling closed-loop temperature stabilization between 2–4 K.

All actuator electronics are housed in a 2U rack enclosure outside the target cave. The system includes stepper motor drivers (Applied Motion ST5-S), a 5 V supply for potentiometers, and an MCC USB-202 ADC for position readout. The enclosure passed Fermilab Operational Readiness Clearance (ORC) review, ensuring compliance with laboratory electrical safety standards. Because of the 70 m separation between the control room and target area, RS232 and USB interfaces were extended via USB-to-Ethernet converters.

The remote operation of the control valves, coupled with a PID control system, maintains temperature stability during thermal equilibrium measurements. This instrumentation arrangement enables continuous monitoring of the helium system while protecting sensitive electronics from the high-radiation environment within the target cave. Online monitoring through PHP-based web interfaces is deployed to monitor the measurement stability during operation.

J. Summary of System Specifications

This concludes the design overview and specifications. Table II summarizes the above sections. The design requirements and safety specifications are listed.

III. CODES, STANDARDS, AND LABORATORY REQUIREMENTS

Despite operating near atmospheric pressure, the Spin-Quest refrigerator was systematically evaluated against ASME BPVC, ASME B31.3, and FESHM requirements to address credible hazards such as vacuum excursions and magnet quenches. This section details the compliance basis, including MAWP calculations, relief strategies, and operational safety margins.

Fermilab’s Environment, Safety, and Health Manual (FESHM) [11] requires that pressure vessels either comply with the ASME BPVC or be classified as “Experiment Vessels.” For experiment vessels, stricter requirements apply, including a 0.8 reduction factor on BPVC allowable stresses, mandatory Section IX-qualified weld and braze procedures, and a comprehensive engineering note verifying overpressure protection [11].

Piping systems were designed per ASME B31.3 for Category D helium service [12]. Pressure-vessel calculations followed ASME BPVC Section VIII, Division 1 for MAWP, wall thickness, and material selection. Overpressure protection principles from BPVC Sections VIII and XIII were followed, with parallel-plate vent capacities informed by Fermilab test data and CGA S-1.3 [19].

A. Maximum Allowable Working Pressures

The following details how each component of the refrigerator underwent analysis to obtain accurate pressure margins.

TABLE II: Summary of Key SpinQuest ^4He Evaporation Refrigerator System Specifications.

Component	Key Parameters	Operating Condition	Safety/Relief
Shell + Nose	Vol: 0.79 ft ³ , 304SS + Al 6061-T6	Vacuum: 10^{-3} Torr	FESHM 5033 Exempt
Phase Separator	OD/ID: 6.4"/3.6", 316L SS	Temp: sub-4 K, P: 3 psig	3 psig Relief Valve
U-Tube Jumper	ID: 0.188 in, 316L SS	ΔP : < 0.4 psig	MAWP: 3648 psig
Pump Stack	Capacity: 10,080 m ³ /h @ 0.1 mbar	P _{nose} : 0.1 mbar	N/A
Instrumentation	20 m remote sensing lines	Category D Service	FESHM 5031.1 Compliant

1) *Shell and Nose Assembly*: The shell and nose assembly is exempt from FESHM 5033 structural requirements due to its small volume (0.79 ft³). Nevertheless, ASME BPVC Section VIII calculations were performed to verify safety margins. The limiting component is the thin aluminum 6061-T6 nose window, machined from a solid rod with weld efficiency of, $E = 1$. For a spherical shell segment of radius $R = 1.87$ in and thickness $t = 0.013$ in, the internal pressure MAWP is given by Eq. 2.

$$P = \frac{SEt}{R - 0.6t} \quad (2)$$

Using ASME Section II [12], Part D allowable stress $\sigma = 15.8$ ksi and weld efficiency $E = 1.0$ for a solid rod, the calculated MAWP is 109.7 psig. Calculating the stress caused by this MAWP with Eq. 3, we obtain 2.1 ksi, which is less than the allowed stress by a factor of 7.

$$\sigma = \frac{PR}{t} \quad (3)$$

The maximum allowable external pressure was also evaluated using UG-28, yielding $P_a = 8.22$ psig from Eq. 4.

$$P_a = \frac{2AE}{3(D_0/t)} \quad (4)$$

Since the magnet relief valve opens at 1 psig, both internal and external margins demonstrate compliance and safe operation.

2) *Phase Separator*: As the separator is connected to the magnet dewar, its MAWP was calculated to ensure system integrity. The helium separator is a welded 304 stainless steel vessel with a wall thickness of ~ 0.065 in. Code evaluation using the ASME VIII thin-shell formula with weld efficiency $E = 0.85$ yields a very high theoretical MAWP of 878.1 psig from Eq. 2. Following the same procedure above, we find that the allowable stress of 50 ksi is much higher than the maximum stress of 2.4 ksi. A functional relief valve set at 3 psig provides a large margin against credible transients while ensuring compliance with FESHM guidance for sub-15 psig operation at the device level. Relief sizing is discussed in more detail in Section III-B

3) *Piping and Tubing (ASME B31.3)*: All helium service lines are designed in accordance with ASME B31.3 for Category D fluid service (nonflammable, nontoxic helium) [12]. Minimum wall thickness requirements are exceeded, and allowable stresses are well above maximum credible loads. Where KF vacuum hardware is used, vendor specifications

TABLE III: MAWP Analysis for Separator-Associated Piping and Tubing.

Service	Material	OD (in)	Wall (in)	MAWP (psig)
Vent to Relief	316L	0.50	0.035	2,279
U-Tube Fill	316L	0.188	0.016	2,872
Fill Line	304	0.435	0.020	1,620
Drain Line	304	0.065	0.0075	4,800
Lower HX	Cu	0.125	0.0125	1,275
He Bypass	304	0.125	0.0175	6,222
Vent to Pumpout	Cu	0.125	0.0125	1,275
Vent Header	304	0.865	0.0675	2,959

rated at ≥ 15 psig are verified. Table III summarizes separator-connected runs, demonstrating large margins relative to NOP conditions.

Table IV summarizes MAWP and normal operating pressure (NOP) for components with potential pressure relevance. For example, the refrigerator bellows have a burst strength of 104 psig while operating at ~ 14.7 psia. These values confirm that normal operation remains well within code-prescribed margins.

TABLE IV: Maximum allowable working pressure (MAWP) and normal operating pressure (NOP) for refrigerator components.

Component	MAWP (psia)	NOP (psia)	Source
Fridge Bellows	104	13.8	Vendor (KeyHigh)
U-tube	3648	13.8	Cryofab
Separator	2450	13.8	In-house analysis
Nose Window	110	10^{-4}	ASME VIII calc.
Insulating Vacuum	16	10^{-8}	Oxford

B. Relief and Venting Design

Using liquid helium for cooling the refrigerator and the magnet coils exposes the system to potential overpressure scenarios.

- 1) Magnet quench or loss of cryostat insulating vacuum, transferring helium into the separator.
- 2) Return pump trip or close-off, producing boil-off relief only.
- 3) Operator error admitting liquid to a warm separator.
- 4) Insulating vacuum loss around the refrigerator/target region, producing a large heat load.

For vessels operating below 15 psig, non-code relief devices may be employed if their function and capacity are demonstrated. Vacuum vessels are addressed under FESHM 5033,

which provides engineering guidance for non-code shapes, requires design-by-analysis, and recommends API 520 and CGA S-1.3 methods for venting calculations. With this in mind, the following section covers these scenarios and our solutions to ensure compatibility with the code.

1) *Separator Relief Path:* As the U-Tube connects the separator to the magnet dewar, the separator could experience a slight increase in helium vapor. However, there is a 5 in SCH 10S relief pipe with a 5 psig parallel plate relief for the 1681 g/s flow, combined with three 15 psig rupture disks. The relief sizing for the separator and magnet dewar was done in a previous internal note [20][21], with the main focus being on when the magnet quenches. Due to the small diameter of the U-Tube, this flow is heavily restricted compared to the magnet relief path. The mass flow in the U-tube can approach 0.5g/s, which is conservatively rounded up to 2kg/h. This results in the following pressure drop of 0.37 psig using Eq. 5

$$\Delta P_{U-Tube} = K_{U-Tube} \frac{\rho_{100} V_{U-Tube}}{2} \quad (5)$$

Here, it is assumed that the helium vapor from the superconducting magnet quench and IV loss is 100 K. Under a quench with insulating vacuum (IV) loss, the magnet vessel is at 29.696 psia [20], and the U-tube connects this vessel directly to the separator vessel that sits at 1 atmosphere or below. This indicates that the separator vessel can never exceed 15 psi under normal operation or the worst failure mode of the magnet. The focus is then placed on the failure mode in which the separator loses the IV around it.

Expansion of cryogenic fluid in the refrigerator during a loss of vacuum event can result in higher-than-normal pressure in the refrigerator. The refrigerator is assumed to be in operation or in standby at the start of a loss of IV. In an IV loss event, the refrigerator shell is warmed up, and the liquid helium in the bottom of the nose will evaporate. During this time, the separator is surrounded by the boil-off of helium. The nose normally holds less than 2 liters, but could hold as much as 6 liters. It is conservative to assume during an IV loss, a temperature of LN², 77K, for the escaping helium from the separator as the relief path of the helium in the nose passes over the separator. The resulting heat flux assumed in a loss-of-vacuum event is $8 \frac{kw}{m^2}$. This is a conservative estimate for the refrigerator space filled with boil-off gas from the cryostat.

It is conservative to assume that the helium in the first stage of the relief line of the separator is at 100K. For the second stage of the separator relief line, it is assumed that the helium has reached 300K. As the separator is an enclosed volume within the refrigerator space, it has a dedicated relief path. This relief path consists of a short inlet stub, a Circle Seal MD520T1-2M-3 relief set at 3 psig, and a ~0.395 in ID run to atmosphere. A total pressure drop from the relief, piping, and U-Tube was calculated at 12 psig [22]. This, according to the FESHM [11], removes the pressure vessel classification.

2) *Common Vent/Header:* The separator and magnet cryostat vents into a large shared header protected by parallel-plate reliefs. Fermilab AD/Cryo capacity tests confirm these devices

provide capacity consistent with CGA S-1.3 guidelines, with sufficient margin for worst-case vacuum jacket failure events.

The 3 psig separator relief provides functional protection, while the vent header reliefs and magnet relief valves provide system-level protection. In accordance with FESHM [11], all sub-15 psig relief devices are capacity-tested or analytically justified and documented.

The final relief is for the U-Tube, which protects the vacuum insulation. The vacuum valve acts as a positive pressure relief valve that protects the system from unlikely scenarios of if helium were to enter the vacuum space.

C. Fabrication and ODH Controls

All welded components were fabricated by ASME-certified welders. Leak integrity was verified by helium mass spectrometer testing, achieving a minimum leak rate of 9.8×10^{-9} std cm³/s. Because cryogenic helium systems present an oxygen-deficiency hazard (ODH), the refrigerator area is equipped with oxygen monitors, alarms, and ventilation. ODH classification and mitigation followed FESHM 5064 [11], and SpinQuest personnel are trained in Fermilab ODH procedures. With the safety and design requirements addressed, testing of the refrigerator can be done.

IV. COMMISSIONING PERFORMANCE (JULY 2024)

The refrigerator was commissioned in spring 2024 to evaluate environmental heat load, cooling capacity, and operational stability. During initial measurements, the fridge pressure was set to 23.48 Torr ($T \approx 2.0$ K) using the gate valve bypass PID control. With the run valve closed and the gate valve bypass fully open, the refrigerator stabilized at a main flow of 5 SLM (Fig. 9).

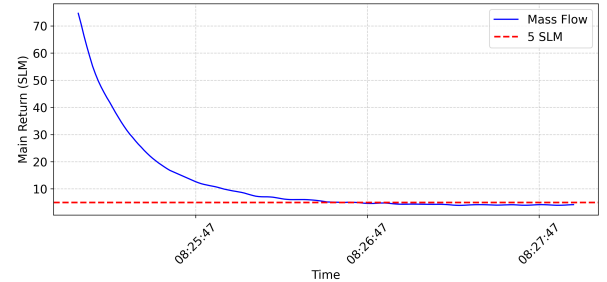


Fig. 9: Steady-state boil-off flow reached after cooling down the system from atmospheric pressure. It is shown that the flow trends towards ~5 SLM at 1.36 Torr, corresponding to an estimated heat load of ~0.3 W from just the environment. During this measurement, the gate valve bypass was open, making this result an upper limit.

Applying the empirical scaling for helium boil-off at 4 K ($1 \text{ W} \approx 17 \text{ SLM}$ from Eq. 6) yields an upper-limit estimate for the environmental heat load of approximately 0.3 W.

$$\dot{Q}_{\max} = \dot{n}_{\max} L^0 \quad (6)$$

As the gate valve was open during this measurement, this result acts as an upper limit of the heat load. The result was

expected to be low due to the high insulation of the baffles and separator.

During beam operations, the high-intensity (10^{13} protons per 4-second spill at 120 GeV), beam to the SpinQuest target cave was delivered. The refrigerator and associated cryostat maintained stable flows throughout data taking, with a measurable periodic increase in heat load attributable to beam interactions as shown in Fig. 10.

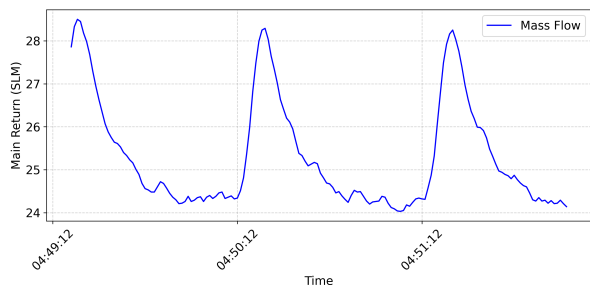


Fig. 10: Main-flow stability under high-intensity beam operation. The main flow shows a spike of ~ 4 SLM every minute, which corresponds to the beam pulse. This added heat load is estimated to be $\sim .2$ W at 4K.

Every 60-second spill, a spike of ~ 4 SLM was measured, giving us an estimated heat load of $\sim .2$ W at 4K.

Thermal equilibrium calibration measurements were first recorded on a CH_2 target insert that was filled and loaded into the cryostat. The Roots boosters were disabled, leaving only the backing pump to operate, and the outflow was regulated by the gate valve bypass actuator under PID control at 20 Torr. Fig. 11 shows stabilization of the temperature within 20 minutes.

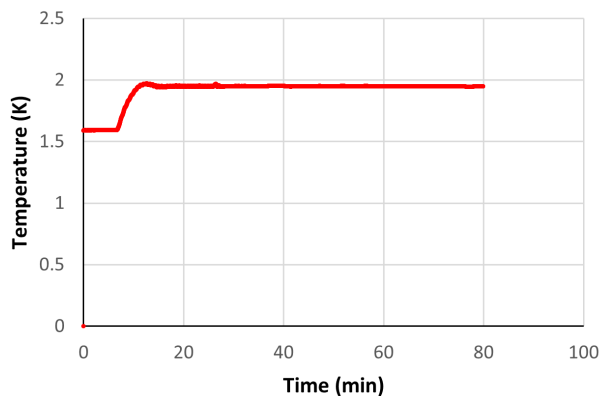


Fig. 11: Temperature profile during thermal equilibrium measurement. NMR area stability was reached in ~ 20 minutes.

This measurement will allow an NMR calibration constant, which will be used in future publications.

The three-month commissioning campaign included multiple soft quenches and one hard quench of the magnet. These quenches are when spikes in the magnet current remove

superconductivity and cause rapid helium expansion. No failures of the refrigerator were observed. Continuous operation demonstrated that the gate valve bypass provided stable control of helium pressure and enabled repeated TE measurements. During enhancement (microwaves on/polarizing) ~ 1 K temperatures were maintained even with over 90% polarization. Fig.12 shows an initial heat load from the microwave of ~ 2.3 W that tapers downward to $.7$ W as the gate valve bypass opens.

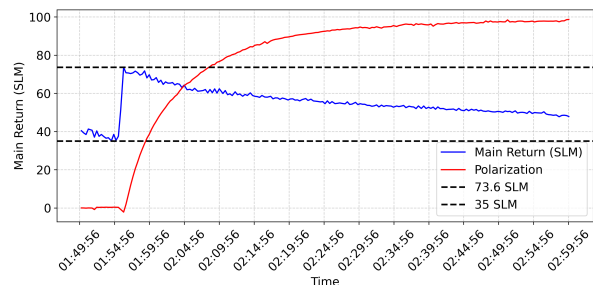


Fig. 12: Polarizing NH_3 to over 90% to determine the effect of the microwave on the cooling power. Once the enhancement starts, a spike of 38.6 SLM can be seen in the main flow. This spike represents a added heat load of ~ 2.3 W and stabilizes to a flow of ~ 47 SLM or $.7$ W.

This added heat load is consistent with the known power of the microwave source. Subsequently, an attenuator was installed, which reduced the observed flow increase during polarization to approximately 20 SLM, corresponding to a microwave heat load of ~ 1.2 W (Fig. 13).

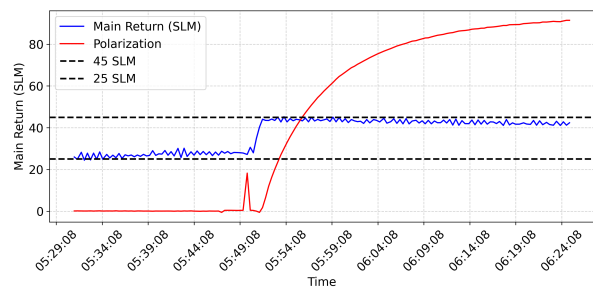


Fig. 13: The flow increase is less after the addition of an attenuator. The flow increase is ~ 20 SLM, which is estimated to be ~ 1 W of cooling power at 4K.

From atmosphere, the fridge takes 26 seconds to reach a helium vapor pressure of 20 Torr, 1 minute and 58 seconds to reach a helium vapor pressure of 3.35 Torr. The total cooldown takes 4 minutes and 14 seconds to stabilize at 1.3 Torr as shown in Fig. 14.

Stable polarization of solid-state NH_3 was achieved, and magnet quench tests were performed during the commissioning, both of which results will be reported separately. With the results stated in the above sections, the experimental total heat load of the system is a maximum of 1.5 W under the

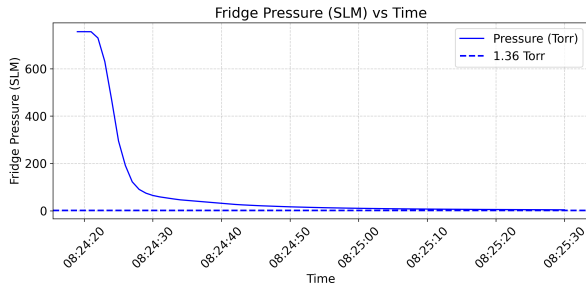


Fig. 14: The total cooldown of the fridge from atmosphere to 1.3 K and 1.3 Torr. The total time took 4 minutes and 14 seconds to cooldown from atmospheric pressure.

maximum testing conditions. This estimate changes based on the beam and microwave stability. However, this heatload, primarily from the microwave, is manageable at flow rates of ≥ 20 SLM PID controlled by the radiation-hardened control valves. This gives an estimated cooling power of ~ 1 W at 4K, a preference that was established to minimize the helium exhausted. A higher flow can be obtained with a measured ≥ 70 SLM, but this increases the helium used. This yields an estimated $\geq \sim 4$ W at 4K which is an improvement from the prior evaporation refrigerators.

V. COMPLIANCE TRACEABILITY MATRIX

The refrigerator design was systematically evaluated against applicable codes and Fermilab safety standards. Several internal notes [22][23][21][24][25], detailed each calculation in detail to Fermilab's standard. Table V below summarizes the refrigerator compliance.

TABLE V: Compliance Traceability Matrix

Standard	Application in Refrigerator Design
ASME B31.3	Tubing and piping design (Category D); material allowables (Table A-1); minimum wall thickness (Para. 304.1.2).
ASME BPVC VIII-1	MAWP calculations for vessels (UG-27, UG-28, UG-34); welding qualifications (Section IX); overpressure protection principles (UG-125–UG-137).
FESHM 5031	Experiment-vessel classification; 0.8 safety factor on allowables; acceptance of sub-15 psig relief devices.
FESHM 5031.1	Documentation thresholds and exemptions for cryogenic piping.
FESHM 5033	Vacuum-vessel safety analysis; venting guidance (referencing API 520 / CGA S-1.3).

VI. CONCLUSIONS

The SpinQuest ^4He evaporation refrigerator satisfies ASME and FESHM requirements with substantial safety margins. Key protective features include the short inlet path to the 3 psig separator relief, large-ID discharge piping, and a high-capacity parallel-plate valve on the common vent. These ensure protection against loss-of-vacuum and quench scenarios while accommodating unusually high instantaneous heat loads in a radiation environment.

Commissioning results confirmed robust performance: stable cooling at $\sim 1\text{--}4$ W, reliable recovery after multiple quenches, and successful thermal equilibrium measurements. Compared to prior $\sim 1\text{--}3$ W refrigerators, this represents an increase in available cooling power needed to combat the higher energy beam from Fermilab. The total heatload managed by the system at a maximum of 1.5 W, which depends on beam and microwave stability. This potential dynamic heat load can be managed by increasing the flow rate and helium used. This factor is mitigated with the use of radiation-hardened PID control valves, which manage the main flow. The refrigerator has been formally approved for operation at Fermilab, and the separator received ASME code stamping. In late 2024, SpinQuest was mentioned during a Fermilab User conference for its safe practices and was used as an example for future labs. Future work will focus on refining control algorithms, enhancing monitoring, and extending long-term stability studies to support SpinQuest polarization campaigns. We aim to apply this process to other experiments and potentially a Helium 3 evaporation refrigerator in the future. Current preparations are underway for the next run of beam.

ACKNOWLEDGMENTS

We thank the Fermilab AD/Cryo group and the SpinQuest target team for engineering reviews, test data, and operations support. This work was supported by the U.S. Department of Energy, Office of Nuclear Physics, Contract No. DE-FG02-96ER40950.

REFERENCES

- [1] A. Abragam and M. Goldman, "Principles of dynamic nuclear polarisation," *Reports on Progress in Physics*, vol. 41, pp. 395–467, 1978, printed in Great Britain.
- [2] A. Abragam, M. Borghini, P. Catillon, J. Coustham, P. Roubeau, and J. Thirion, "Diffusion de protons polarisés de 20 mev par une cible de protons polarisés et mesure préliminaire du paramètre cnn ," *Physics Letters*, vol. 2, no. 7, pp. 310–311, 1962. [Online]. Available: <https://www.sciencedirect.com/science/article/pii/0031916362901221>
- [3] A. Abragam and C. S. . G. sur Yvette (France), "A new principle in nuclear resonance. applications," 1958. [Online]. Available: <https://inis.iaea.org/records/503js-9bm91>
- [4] M. Borghini, "Nuclear spin relaxation and dynamic polarization versus electron spin-spin relaxation," *Physics Letters A*, vol. 26, no. 6, pp. 242–244, 1968. [Online]. Available: <https://www.sciencedirect.com/science/article/pii/0375960168906269>
- [5] —, "Spin-temperature model of nuclear dynamic polarization using free radicals," *Phys. Rev. Lett.*, vol. 20, pp. 419–421, Feb 1968. [Online]. Available: <https://link.aps.org/doi/10.1103/PhysRevLett.20.419>
- [6] S. Bültmann *et al.*, "A study of lithium deuteride as a material for a polarized target," *Nuclear Instruments and Methods in Physics Research Section A: Accelerators, Spectrometers, Detectors and Associated Equipment*, vol. 425, no. 1, pp. 23–36, 1999. [Online]. Available: <https://www.sciencedirect.com/science/article/pii/S0168900298013412>
- [7] C. Keith *et al.*, "A polarized target for the clas detector," *Nuclear Instruments and Methods in Physics Research Section A: Accelerators, Spectrometers, Detectors and Associated Equipment*, vol. 501, no. 2, pp. 327–339, 2003. [Online]. Available: <https://www.sciencedirect.com/science/article/pii/S0168900203004297>
- [8] D. G. Crabb *et al.*, "High-precision measurement of the analyzing power in large- p_{\perp}^2 spin-polarized 24-gev/c proton-proton elastic scattering," *Phys. Rev. Lett.*, vol. 65, pp. 3241–3244, Dec 1990. [Online]. Available: <https://link.aps.org/doi/10.1103/PhysRevLett.65.3241>

- [9] F. Z. Khiari *et al.*, “Acceleration of polarized protons to 22 gev/c and the measurement of spin-spin effects in $p_{\uparrow}+p_{\uparrow}\rightarrow p+p$,” *Phys. Rev. D*, vol. 39, pp. 45–85, Jan 1989. [Online]. Available: <https://link.aps.org/doi/10.1103/PhysRevD.39.45>
- [10] J. Pierce *et al.*, “Dynamically polarized target for the g2p and gep experiments at jefferson lab,” *Nuclear Instruments and Methods in Physics Research Section A: Accelerators, Spectrometers, Detectors and Associated Equipment*, vol. 738, pp. 54–60, 2014. [Online]. Available: <https://www.sciencedirect.com/science/article/pii/S0168900213016999>
- [11] Fermilab, “Fermilab es&h manual (feshm) chapters 5031, 5031.1, and 5033,” Fermi National Accelerator Laboratory, Tech. Rep., 2025, internal Fermilab code.
- [12] ASME, *BPVC Section VIII: Rules for Construction of Pressure Vessels, Division 1*. New York, NY: American Society of Mechanical Engineers, 2015.
- [13] R. C. Gentzlinger and K. E. Christensen, “A guideline for design, analysis, and fabrication of vacuum vessels for cryogenic accelerators,” Los Alamos National Laboratory, Tech. Rep., 1991. [Online]. Available: <https://cds.cern.ch/record/902556>
- [14] N. Baltzell *et al.*, “The clas12 beamline and its performance,” *Nuclear Instruments and Methods in Physics Research Section A: Accelerators, Spectrometers, Detectors and Associated Equipment*, vol. 959, p. 163421, 2020. [Online]. Available: <https://www.sciencedirect.com/science/article/pii/S0168900220300267>
- [15] C. Keith, “Polarized solid targets at jefferson lab,” in *Proceedings of the 16th International Workshop on Polarized Sources, Targets, and Polarimetry (PSTP 2015)*. Bochum, Germany: SISSA, Sep. 2015, p. 013, published: Dec. 2, 2015.
- [16] J. Benesch *et al.*, “Jefferson lab hall c: Precision physics at the luminosity frontier,” 2022. [Online]. Available: <https://arxiv.org/abs/2209.11838>
- [17] T. O. Niinikoski, *The Physics of Polarized Targets*. Cambridge University Press, 2020.
- [18] T. Niinikoski, “Construction of sintered copper heat exchangers,” *Cryogenics*, vol. 11, no. 3, pp. 232–233, 1971. [Online]. Available: <https://www.sciencedirect.com/science/article/pii/0011227571903195>
- [19] Compressed Gas Association, “Pressure relief device standards, part 3,” Fermi National Accelerator Laboratory, Tech. Rep., 2020, internal Fermilab Note.
- [20] E. Voirin and D. Keller, “E1039 target cryostat relief system analysis,” Fermi National Accelerator Laboratory, Tech. Rep., 2021, internal Fermilab Note.
- [21] R. L. S. and D. Keller, “E1039 separator relief calculations,” Fermi National Accelerator Laboratory, Batavia, IL, Tech. Rep., 2022, internal engineering note.
- [22] University of Virginia Spin Group, “Uva evaporation refrigerator: E1039 pressure vessel note — target vacuum vessel,” Fermi National Accelerator Laboratory, Batavia, IL, Tech. Rep., 2020, rev. 8/12/21, internal engineering note.
- [23] M. White, “Ad/cryo parallel plate capacity calculation (ed0003987),” Fermi National Accelerator Laboratory, Batavia, IL, Tech. Rep., 2016, internal engineering note.
- [24] T. G. and D. Keller, “E1039: Lhe relief analysis for uva refrigerator phase separator,” Fermi National Accelerator Laboratory, Batavia, IL, Tech. Rep., 2020, internal engineering note.
- [25] R. L. S. and D. Keller, “Manometer line pressure safety,” Fermi National Accelerator Laboratory, Batavia, IL, Tech. Rep., 2022, internal engineering note.